ROYAL SOCIETY
OF **CHEMISTRY**

15 YEARS
ANNIVERSARY

Chemical Science

Check for updates

Molecular engineering of bis(triphenylamine)-modified fluorene luminophore for immensely enriching anisotropic force-triggered high-contrast tricolor fluorescent molecular switches library†

Zhao Chen, [ID] *[a] Yijie Zou,[a] Ya Yin,[b] Diandian Deng,[d] Yue Yang,[c] Congbin Fan, [ID] [a] Shouzhi Pu [ID] *[a] and Gang Liu [ID] [a]

The preparation of anisotropic mechanical force-triggered high-contrast tricolor fluorescent solid switches is both significant and extremely challenging. Herein, we report a high-efficiency molecular engineering strategy for developing mechanochromic compounds that exhibit an infrequent yet contrasting three-color fluorescence switching feature. Notably, 14 new symmetric fluorescent molecules by introducing a variety of substituents on either side of the central organic moiety involving 4,4′-((9H-fluoren-9-ylidene)methylene)bis(N,N-diphenylaniline) are successfully obtained, and 10 new fluorogenic compounds have been discovered to exhibit seldom-observed tricolored mechanofluorochromic phenomena. Impressively, among them, 8 luminogens demonstrate exceptionally scarce anisotropic force-triggered high-contrast three-color fluorescence responses, which is a commendable achievement, fully verifying the effectiveness of our molecular engineering strategy presented in this study. Furthermore, based on two newly developed representational mechanically responsive tricolor fluorescence switches, three advanced information anticounterfeiting systems are skillfully constructed.

Introduction

Mechanically responsive emissive molecular switches, featuring fluorescence color alteration driven by an anisotropic mechanical force, are an important class of functionalized materials.[1–11] Such intelligent materials have garnered considerable attention from researchers due to their potential in information storage, mechanical sensing, and safety technology fields.[12–23] Over the past two decades, several force-triggered fluorescent solid switching systems have been exploited.[24–30] In these reports, a majority of luminogens exhibit bicolor fluorescence responses upon stimulation by mechanical force.[31–36] In contrast, tricolor fluorescence switches, especially those featuring three high-

contrast fluorescence colors induced by anisotropic force, remain relatively scarce. Thanks to the endeavors of scientific researchers in the field of force-responsive smart emissive materials, some mechanical force-activated molecular switches characterized by noticeable tricolor fluorescence changes have been developed. For example, in 2013, Ma *et al.* reported a fluorogenic compound consisting of one tetraphenylalanine spacer and two chromophores of rhodamine B and pyrene, and this luminogen displayed a blue-to-bluish-green-to-reddish three-color mechanofluorochromism.[37] Guo *et al.* prepared a propeller-type squaraine dye in 2023, and the yellow fluorescence of the as-synthesized dye turned into orange and deep red after slight and heavy grinding, respectively.[38] Our group made a valuable contribution to this promising science field in 2024 when we successfully developed the first example of tricolor mechanofluorochromic luminogen with hypso- and bathochromic bidirectional high contrast beyond 120 nm.[39] However, the production of this kind of force-responsive tricolor fluorogenic switch heavily relies on accidental findings, and preparing more tricolored fluorescence solid switches induced by anisotropic grinding *via* universal molecular design principles is very urgent and encounters severe challenges.

Molecular engineering strategy, which involves precise control of molecular properties by manipulating substance structures, represents a high-efficiency scientific approach for

[a] Jiangxi Provincial Key Laboratory of Organic Functional Molecules, Institute of Organic Chemistry, Jiangxi Science and Technology Normal University, Nanchang 330013, P. R. China. E-mail: 1020160936@jxstnu.edu.cn; pushouzhi@tsinghua.org.cn

[b] State Key Laboratory of Coordination Chemistry, School of Chemistry and Chemical Engineering, Nanjing University, Nanjing 210023, P. R. China

[c] College of Chemistry, Jilin University, Changchun 130012, P. R. China

[d] School of Chemistry and Molecular Engineering, East China Normal University, Shanghai 200241, P. R. China

optimizing material functionalities at the molecular level. This strategy has significant advantages in the development of high-performance functionalized materials.[40–45] Indeed, numerous functionalized luminogenic molecules with rare photophysical properties have been successfully prepared using a molecular engineering strategy.[46–51] Representatively, in 2016, Seki *et al.* produced 48 mononuclear gold(ɪ) complexes through the strategy of substituent engineering, and a new mechanolumi-nochromic gold(ɪ) complex featuring the unusual force-induced crystal-to-crystal phase transition was screened out.[52] Herein, we present an effective molecular engineering strategy involving isomeric and substituent engineering to discover fluorogenic compounds with desired anisotropic mechanical force-induced high-contrast tricolor fluorescence changes. More specifically, by introducing substituents with different electronic effects or isomeric substituents to the two sides of the central organic moiety 4,4′-((9H-fluoren-9-ylidene)methylene)bis(N,N-diphenylaniline), 15 symmetric fluorescence compounds are obtained. Triphenylamine is an outstanding aggregation-induced emission (AIE) building block, and the presence of two triphenylamine groups not only contributes to the achievement of high-brightness solid-state fluorescence of 15 targets **Sym-Pos-R** compounds but also endows their highly twisted molecular conformations of these luminogens that provide the possibility for achieving unusual anisotropic force-induced three-color fluorescence responses. As for two benzene units substituted with diverse electron-effect groups on both sides of a central moiety, their electron-donating or electron-withdrawing effect and the electron-donating effect of two triphenylamine units successfully build the symmetric donor–donor–donor (D–D–D) or acceptor–donor–acceptor (A–D–A)-type fluorogenic molecular systems. The intramolecular charge transfer characteristics of these D–D–D or A–D–A luminogens are susceptible to external mechanical stimulation. Therefore, these fluorogenic compounds are expected to exhibit attractive mechanical force-dependent fluorescence behaviors. Furthermore, methoxy, N,N-dimethyl, trifluoromethyl, nitro, or chlorine groups may trigger the appearance of intermolecular C–H⋯O, C–H⋯N, C–H⋯F or C–H⋯Cl interactions, which serve as the critical factor for realizing interesting mechanofluorochromic phenomena. Additionally, the relative conformation of two substituted benzene groups on both sides of the fluorene unit may vary upon force stimulation, which may lead to a significant alteration in the physical molecular packing mode of luminogen and thus achieve high-contrast mechanochromic fluorescence. Indeed, 11 three-color mechanofluorochromic molecules are discovered (Fig. 1a). Remarkably, among them, 9 luminogens exhibit high-contrast tricolored fluorescence responses under the stimulation of anisotropic force, including our previously reported luminogen **Sym-o-CF₃**.[39] From the newly discovered 8 contrasting three-color mechanofluorochromic compounds, two representative luminogens **Sym-p-OMe** and **Sym-m-OMe**, which involve force-induced gradually bathochromic and hypso- and bathochromic bidirectional fluorescence changes respectively, are selected for anticounterfeiting applications. Three different modes of advanced information encryption systems are elaborately constructed.

Results and discussion

The five target compounds **Sym-p-OMe**, **Sym-p-NMe₂**, **Sym-p-CF₃**, **Sym-p-NO₂**, **Sym-p-Cl** were firstly synthesized in high yields *via* substituent engineering strategy, which involved introducing *para*-substituted benzene units with various electronic effects on both sides of the 4,4′-((9H-fluoren-9-ylidene)methylene)bis(N,N-diphenylaniline) moiety. Subsequently, the remaining ten target molecules, **Sym-m-OMe**, **Sym-m-NMe₂**, **Sym-m-CF₃**, **Sym-m-NO₂**, **Sym-m-Cl**, **Sym-o-OMe**, **Sym-o-NMe₂**, **Sym-o-CF₃**, **Sym-o-NO₂**, and **Sym-o-Cl**, were also smoothly obtained in good yields through the strategy of isomeric engineering. The synthetic routes of 15 **Sym-Pos-R** compounds are shown in Scheme S1.†

A high-efficiency screening method was employed to identify rare mechanical force-manipulatable, high-contrast, three-color fluorescent molecular switches from 15 synthesized luminogens. As a first step, the mechanofluorochromic behaviors of the as-prepared 15 **Sym-Pos-R** compounds were evaluated by the photoluminescence (PL) spectroscopic technique. Four of these luminogens showed no solid-state fluorescence changes before and after mechanical grinding (Fig. S1†), and powder X-ray diffraction (PXRD) experimental results confirmed that no morphological changes occurred for unground and ground solid states of **Sym-m-NMe₂**, **Sym-p-NO₂**, **Sym-m-NO₂** or **Sym-m-CF₃** (Fig. S2†). Interestingly, the remaining 11 luminogens all exhibited three-color mechanofluorochromic phenomena. In the following second step, we screened out 9 force-triggered high-contrast tricolor fluorescence switches from 11 tricolored mechanofluorochromic luminogens. A force-dependent emissive switch capable of achieving hypso- and bathochromic bidirectional fluorescence mechanochromisms beyond 120 nm was developed for the first time.[34] The 8 new high-contrast three-color mechanofluorochromic **Sym-Pos-R** compounds were divided into two categories: one is the force-responsive hypso- and bathochromic bidirectional fluorescence switching molecules (category I, Fig. 1b and c); the other is the force-responsive gradually bathochromic three-color fluorescence switching molecules (category II, Fig. 1d–g). The representative luminogens **Sym-m-OMe** and **Sym-p-OMe** from categories I and II compounds were systematically investigated in the third step. As shown in Fig. 2a, the primal **Sym-m-OMe** emitted high-brightness yellow-green solid fluorescence with the maximum emission peak (λ_{max}) at 538 nm, and its absolute fluorescence quantum yield (Φ_F) reached up to 79.33%. In this research, we utilized an anisotropic force as the applied force, which was achieved through manual mechanical grinding. In the field of mechanoluminochromism, mechanical grinding typically denotes heavy grinding and heavy grinding is generally performed in an agate mortar using pestle pressure consistent with average adult manual force. Slight grinding typically refers to the process in which the powder sample is gently agitated using a rod with minimal force applied by an adult. During actual experimental procedures, the operator can gently agitate the powder sample with mild force using a rod to accomplish the process of slight grinding. Subsequently, the heavy grinding
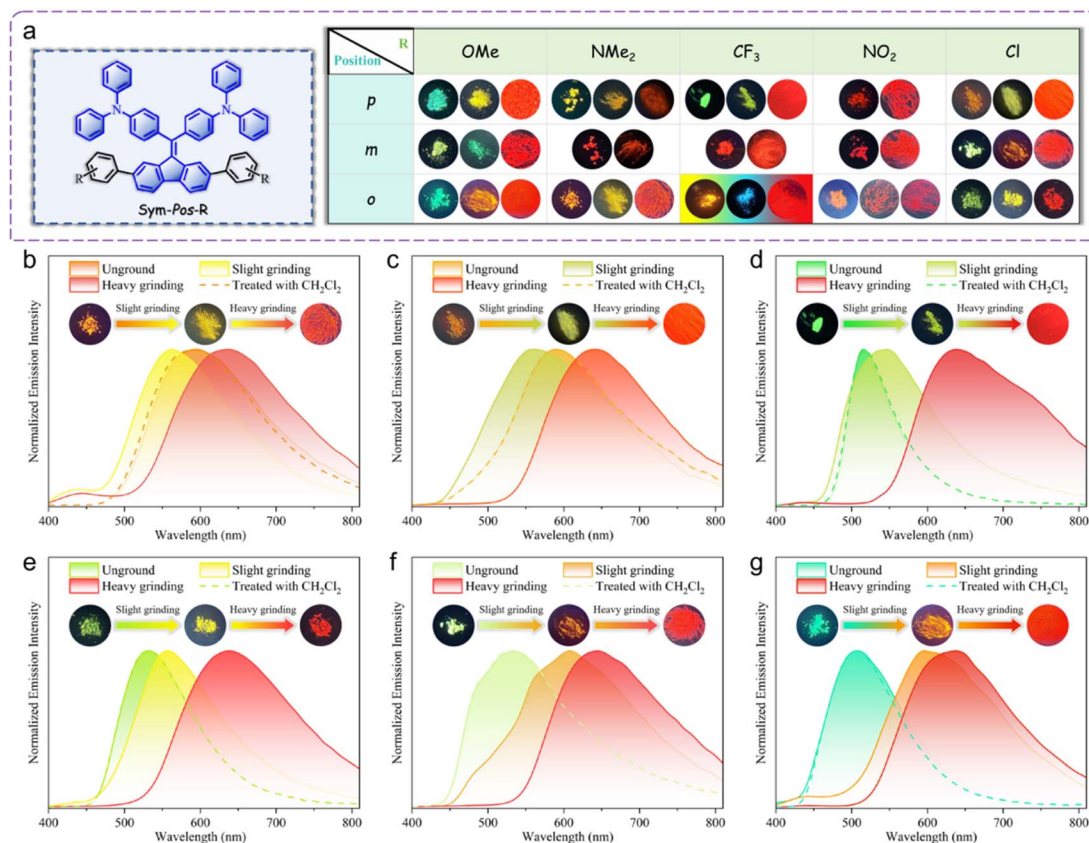
Fig. 1 (a) Molecular structures of the 15 **Sym-Pos-R** compounds. Photographs exhibition of force-triggered fluorescence responses of 15 **Sym-Pos-R** compounds. The leftmost photograph is the fluorescence state of the as-synthesized solid, the middle photograph is the fluorescence state of the slightly ground solid, and the rightmost photograph is the fluorescence state of the heavily ground solid. The three photographs with colored backgrounds demonstrate force-induced three different solid fluorescence states of our previously reported **Sym-o-CF₃**.[39] Normalized PL spectra and PL photographs under 365 nm UV light of the as-synthesized, slightly ground, and heavily ground solid states of **Sym-o-NMe₂** (b), **Sym-p-Cl** (c), **Sym-p-CF₃** (d), **Sym-o-Cl** (e), **Sym-m-Cl** (f), **Sym-o-OMe** (g).

procedure is completed by applying a normal adult manual grinding force. Remarkably, slight grinding triggered a noticeable blue shift of 40 nm for solid **Sym-m-OMe**, and the slightly ground sample displayed clear green fluorescence with the Φ_F value of 62.59%. Interestingly, following heavy grinding, the green light-emitting solid transitioned to a red fluorescent state ($\Phi_F = 34.90\%$), accompanied by a wide-range ($\Delta\lambda_{em,max} = 152$ nm) bathochromic shift. Therefore, **Sym-m-OMe** belonged to a yellow-green-to-green-to-red bidirectional high-contrast mechanofluorochromic molecule. Similarly, an anisotropic force-manipulatable orange-to-yellow and yellow-to-red bidirectional high-contrast fluorescence switching phenomenon was also witnessed for **Sym-o-NMe₂** (Fig. 1b) or **Sym-p-Cl** (Fig. 1c).

The mechanical force-caused fluorescence responses of **Sym-p-OMe** were demonstrated in Fig. 2d, and the as-synthesized sample of **Sym-p-OMe** displayed a strong green emission ($\Phi_F = 81.44\%$) with a λ_{max} at 504 nm. Excitingly, after light grinding using a spatula, an apparent change in the fluorescence color from green to yellow was noticed. Its yellow fluorescence ($\Phi_F = 78.48\%$) of the slightly ground solid was converted into a red fluorescence ($\Phi_F = 24.23\%$) with a wide-range red shift of the

λ_{max} from 552 nm to 641 nm upon vigorous grinding. Consequently, **Sym-p-OMe** could gradually realize bathochromic high-contrast three-color fluorescence conversions through anisotropic mechanical force. Analogously, **Sym-p-CF₃** (Fig. 1d), **Sym-o-Cl** (Fig. 1e), **Sym-m-Cl** (Fig. 1f), and **Sym-o-OMe** (Fig. 1g) also exhibited gradually bathochromic tricolored mechanofluorochromic behaviors. For the two categories of force-responsive three-color fluorescence switches, their initial solid fluorescence could be recovered upon exposure of their individually ground samples to dichloromethane (CH₂Cl₂) vapor. Furthermore, as demonstrated in Fig. S3,† all 10 newly developed fluorogenic compounds displayed good three-color mechanofluorochromic repeatabilities. Fluorescence parameters of the obtained 14 new **Sym-Pos-R** luminogens in diverse solid states are summarized in Tables 1 and S1,† and the graphs of fluorescence lifetimes of 10 new three-color mechanofluorochromic compounds in various solid states are shown in Fig. S8–S17† and the lifetime curves of their slightly ground solids were not a simple superposition of those of their respective unground and heavily ground solids for these 10 three-color mechanofluorochromic luminogens, which provided support for the fact that these tricolor fluorescent
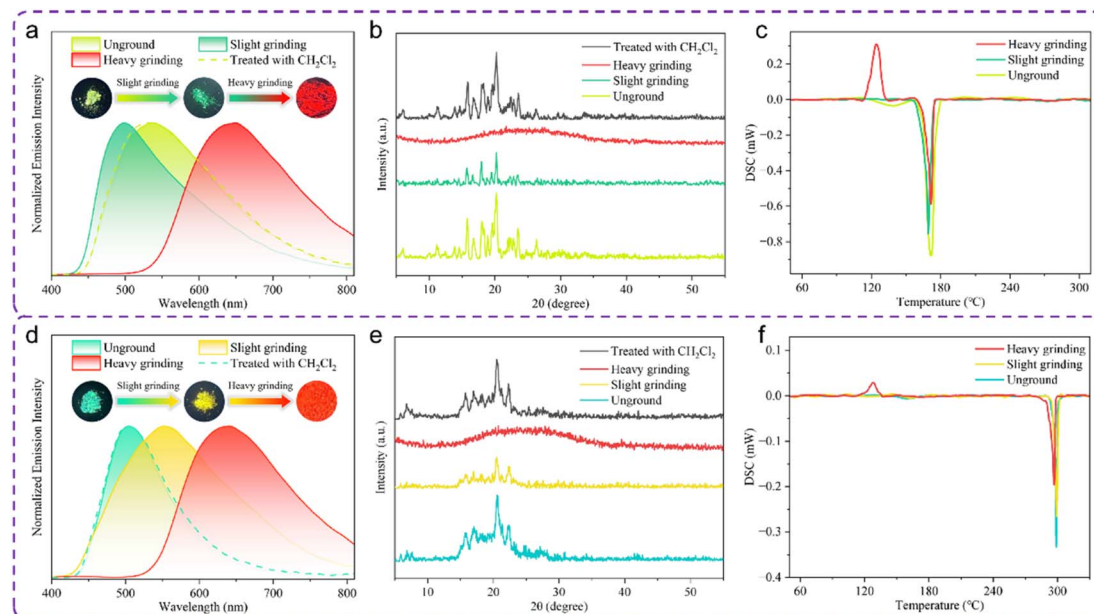
Fig. 2 Normalized PL spectra and PL photographs under 365 nm UV light of the as-synthesized, slightly ground, and heavily ground solid states of **Sym-*m*-OMe** (a), **Sym-*p*-OMe** (d). PXRD patterns of **Sym-*m*-OMe** (b) and **Sym-*p*-OMe** (e) in various solid states. DSC curves of **Sym-*m*-OMe** (c) and **Sym-*p*-OMe** (f) in various solid states. The scan rate is 5 °C min^{-1} under N$_2$.

molecular switches underwent three-color conversion rather than a mixture of two colors under the action of anisotropic force. The Commission Internationale de L'Eclairage (CIE) 1931 chromaticity diagrams of 14 new **Sym-*Pos*-R** luminogens in various solid states are shown in Fig. S4.† Three representative luminogens **Sym-*m*-OMe**, **Sym-*o*-OMe**, and **Sym-*p*-NO₂** were selected to study whether molecular structural changes occurred upon mechanical stimulation. As exhibited in Fig. S5 and S6,† the ¹H NMR spectra of slightly and heavily ground solid samples of **Sym-*m*-OMe** and **Sym-*o*-OMe** matched well with those of their pristine solid samples, respectively. Similarly, the ¹H NMR spectrum of the ground solid sample of **Sym-*p*-NO₂** also matched well with that of the unground solid **Sym-*p*-NO₂** (Fig. S7†). Therefore, no chemical structural change

occurred under anisotropic force stimulation for solid **Sym-*m*-OMe**, **Sym-*o*-OMe**, or **Sym-*p*-NO₂**. PXRD experiments were carried out to elucidate the possible reasons for the tricolor mechanofluorochromic phenomena of categories I and II luminogens.

As can be seen in Fig. 2b and e, the PXRD patterns of the unground solid forms of **Sym-*m*-OMe** and **Sym-*p*-OMe** showed clear and sharp diffraction peaks, indicative of their good crystallinities. After slight grinding, the number and intensity of the pristine diffraction peaks significantly decreased. However, their original crystallinities could be maintained. The synergistic effect involving the loss of crystallinities and conformational variations was likely responsible for the observed slight force-triggered hypsochromically/bathochromically shifted

Table 1 The λ_{max} and Φ_F values of 14 new **Sym-*Pos*-R** luminogens in different solid states

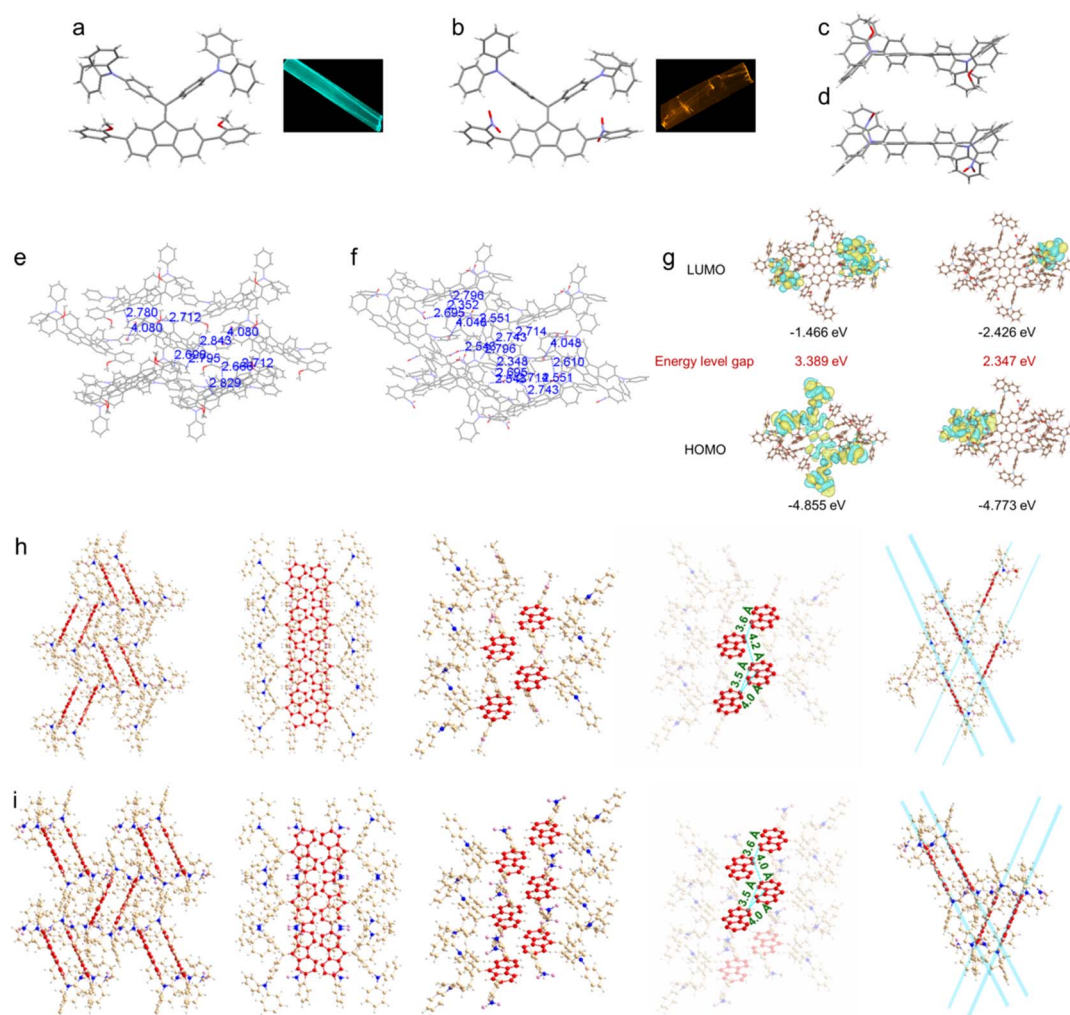| Compound	λ_{max}/nm (unground)	Φ_F (unground)	λ_{max}/nm (slight grinding)	Φ_F (slight grinding)	λ_{max}/nm (heavy grinding)	Φ_F (heavy grinding)
Sym-*p*-OMe	504	81.44%	552	78.48%	641	24.23%
Sym-*m*-OMe	538	79.33%	498	62.59%	650	34.90%
Sym-*o*-OMe	507	65.11%	596	42.19%	638	24.31%
Sym-*p*-NMe₂	553	83.32%	575	71.16%	635	21.00%
Sym-*m*-NMe₂	619	56.32%	—	—	620	51.24%
Sym-*o*-NMe₂	595	21.75%	563	15.17%	636	11.15%
Sym-*p*-CF₃	515	93.46%	547	80.53%	638	33.62%
Sym-*m*-CF₃	643	47.26%	—	—	642	45.36%
Sym-*p*-NO₂	658	15.30%	—	—	656	14.56%
Sym-*m*-NO₂	646	17.85%	—	—	647	15.72%
Sym-*o*-NO₂	611	11.60%	639	9.32%	671	7.08%
Sym-*p*-Cl	590	51.99%	558	47.30%	640	20.53%
Sym-*m*-Cl	533	84.53%	608	78.90%	644	27.27%
Sym-*o*-Cl	532	86.86%	557	79.50%	638	27.05%

Fig. 3 Crystal structure of **Sym-*o*-OMe**: (a) top view. The inset shows the fluorescence photograph of **Sym-*o*-OMe** crystal under 365 nm UV irradiation; (c) side view. Crystal structure of **Sym-*o*-NO₂**: (b) top view. The inset shows the fluorescence photograph of **Sym-*o*-NO₂** crystal under 365 nm UV irradiation; (d) side view. (e) Crystal packing diagram of **Sym-*o*-OMe**. It exhibits weak intermolecular C−H···O, C−H···π and π··· π interactions. (f) Crystal packing diagram of **Sym-*o*-NO₂**. It exhibits weak intermolecular C−H···O, C−H···π and π···π interactions. (g) Energy diagrams and the frontier molecular orbital profiles of **Sym-*o*-OMe** crystal (left) and **Sym-*o*-NO₂** crystal (right) in tetramer forms. Packing modes of blue-green fluorescent **Sym-*o*-OMe** crystal (h) and orange-yellow fluorescent **Sym-*o*-NO₂** (i) under different views. Detailed view of stacking mode of the fluorene planes in adjacent **Sym-*o*-OMe** (h) or **Sym-*o*-NO₂** (i) molecules.

emissions of solids **Sym-*m*-OMe** and **Sym-*p*-OMe**.[53–55] For their PXRD patterns of heavily ground solids **Sym-*m*-OMe** and **Sym-*p*-OMe**, no scattering peaks were noticed, suggesting the formation of amorphous solid phases. Indeed, vigorous grinding could destroy the initial well-order crystalline states of **Sym-*m*-OMe** and **Sym-*p*-OMe** and promote the complete transformation of crystalline to amorphous phases. The observed red fluorescence of heavily ground solid **Sym-*m*-OMe** or **Sym-*p*-OMe** was likely attributed to the molecular conformation and stacking planarization.[34] The observed tricolor mechano-fluorochromic mechanism of the remaining categories I and II compounds was similar to that of **Sym-*m*-OMe** or **Sym-*p*-OMe** (Fig. S18†). Differential scanning calorimetry (DSC) tests were performed to understand further the mechanism of force-responsive tricolored fluorescence transformations of representational categories I/II luminogens **Sym-*m*-OMe** and **Sym-*p*-**

OMe. As presented in Fig. 2c and f, the DSC curves of both unground and slightly ground solid forms of **Sym-*m*-OMe** and **Sym-*p*-OMe** possessed a prominent endothermic peak at approximately 172 °C and 299 °C respectively, and the endothermic peak intensities observed in the DSC curves of unground solids **Sym-*m*-OMe** and **Sym-*p*-OMe** were stronger than those of their slightly ground solid samples. Moreover, an evident broad endothermic peak at 139 °C was noticed in the DSC curve of the as-prepared solid **Sym-*m*-OMe**. These results implied the higher thermostabilities of unground samples **Sym-*m*-OMe** and **Sym-*p*-OMe** compared with their slightly ground solid states. Noticeably, for solids **Sym-*m*-OMe** and **Sym-*p*-OMe**, the cold-crystallization exothermic peaks at 124 °C and 128 °C were observed respectively after heavy grinding, which confirmed the destruction of their original crystalline structures and the formation of amorphous states. Understandably, the
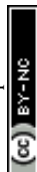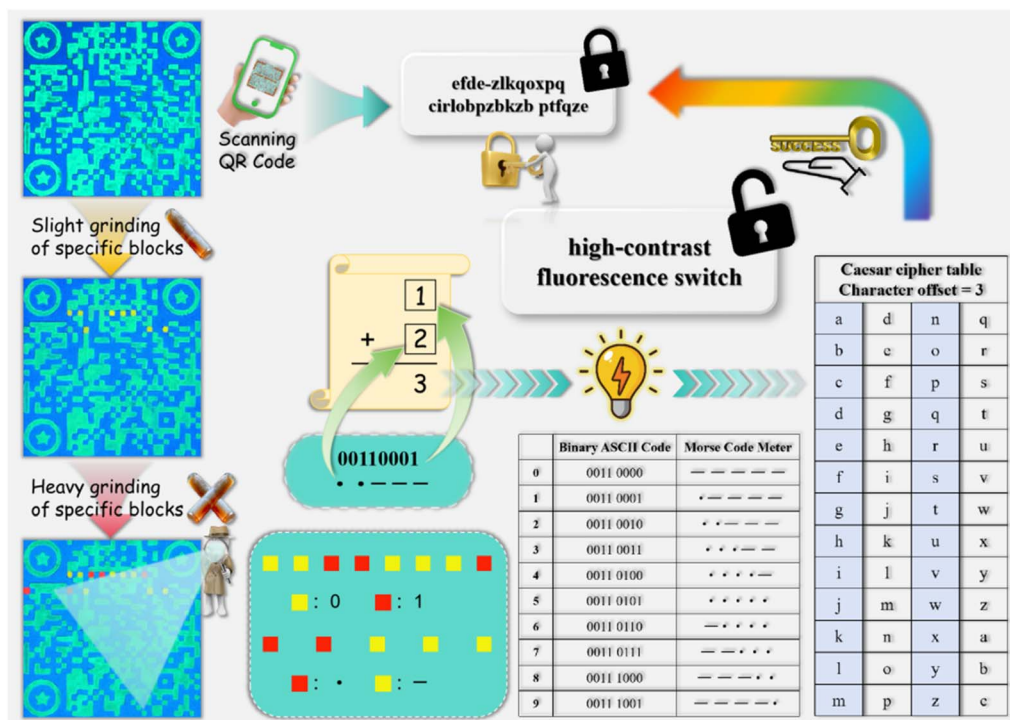
Fig. 4 Schematic diagram of a multilayer anticounterfeiting system based on the colored QR code, binary ASCII code, Morse code, and Caesar cipher applying the three-color mechanofluorochromic effect of **Sym-*p*-OMe**.

high-contrast three-color mechanofluorochromic properties of **Sym-*m*-OMe** and **Sym-*p*-OMe** were associated with a force-induced gradual transition from stable crystalline to meta-stable amorphous states.

High-quality strip-shaped single crystals of **Sym-*o*-OMe** and **Sym-*o*-NO₂** were fortunately obtained by layering poor solvent *n*-hexane on top of a CH_2Cl_2 solution of **Sym-*o*-OMe** or **Sym-*o*-NO₂**. As Fig. 3a–d shows that two triphenylamine groups boost the formation of the highly twisted molecular conformations of

Sym-*o*-OMe and **Sym-*o*-NO₂**. Multiple weak intermolecular C–H⋯O, C–H⋯π and π⋯π interactions are present in the stacking structures of molecules **Sym-*o*-OMe** (Fig. 3e) and **Sym-*o*-NO₂** (Fig. 3f), which provides a basis for the force-dependent molecular conformational changes of **Sym-*o*-OMe** or **Sym-*o*-NO₂**. Taking **Sym-*o*-OMe** as an example, although weak multiple intermolecular C–H⋯O, C–H⋯π and π⋯π interactions facilitate the molecular packing of **Sym-*o*-OMe**, the absence of a strong intermolecular force leads to a loose packing motif of
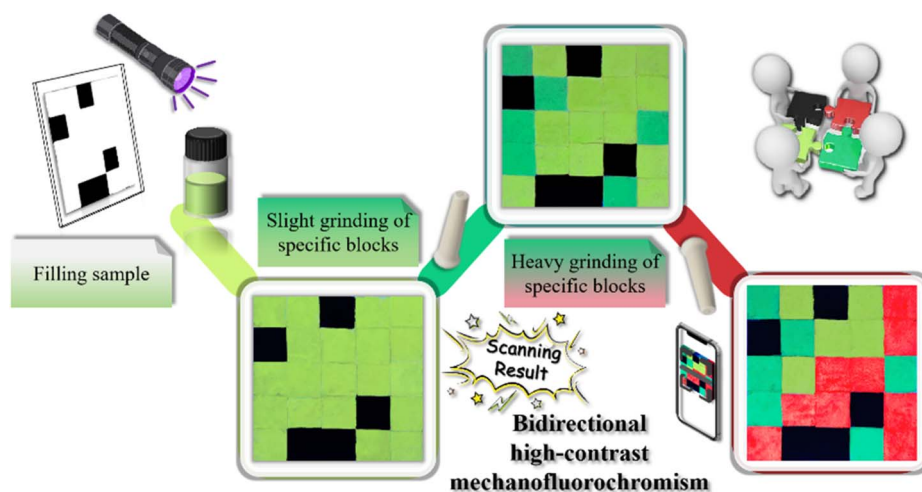

Fig. 5 Schematic diagram of a 3D-colored code-based anticounterfeiting system applying hypso- and bathochromic bidirectional high-contrast mechanofluorochromism of **Sym-*m*-OMe**.
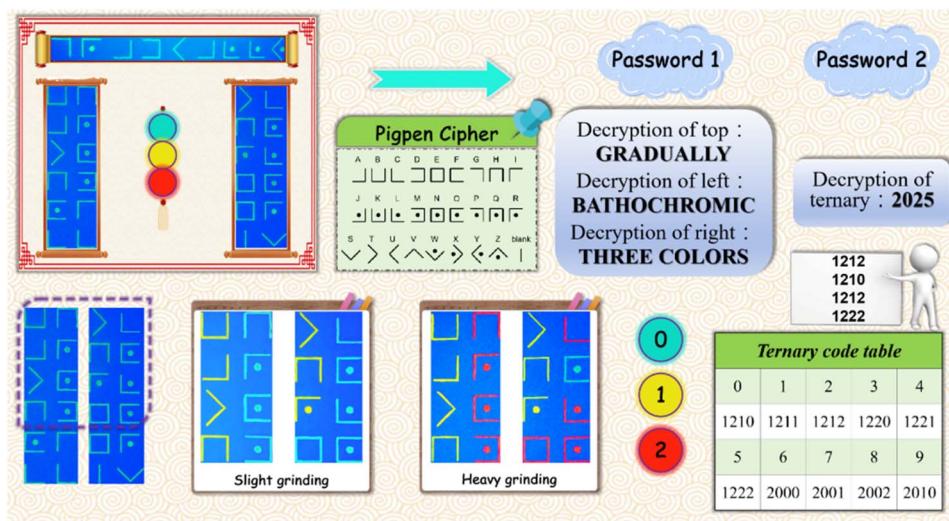
Fig. 6 Schematic diagram of a multilayer anticounterfeiting system based on the pigpen cipher and ternary code applying force-triggered three-color solid fluorescence of **Sym-*p*-OMe**.

Sym-*o*-OMe. Therefore, its ordered crystal packing of **Sym-*o*-OMe** may readily collapse after heavy grinding. As presented in Fig. S19,† upon 365 nm UV irradiation, luminogen **Sym-*o*-OMe** (2.0×10^{-4} mol L^{-1}) in pure CH$_2$Cl$_2$ solution showed obvious yellow-green fluorescence, while almost no fluorescence was noticed for luminogen **Sym-*o*-OMe** (1.0×10^{-3} mol L^{-1}) in pure CH$_2$Cl$_2$ solution. It was possible that the fluorescence quenching was caused by the formation of strong π–π stacking between molecules at high concentrations. Meanwhile, compound **Sym-*o*-OMe** displayed the AIE feature (Fig. S20†), and the PL exhibited by **Sym-*o*-OMe** in the DMF/water mixture with a 90% water fraction was similar to that of heavily ground solid **Sym-*o*-OMe**. As illustrated in Fig. S21,† the planarization of molecular packing mode and enhanced intermolecular π–π interactions were possibly responsible for the red fluorescence triggered by heavy grinding of **Sym-*o*-OMe**, and heavy grinding-triggered planar stacking was related to relatively tight π–π stacking rather than extremely tight π–π stacking, which affected electron transfer and solid-state fluorescence properties. Indeed, the Φ_F value of the heavily ground solid **Sym-*o*-OMe** was lower than that of its corresponding pristine solid sample. Density functional theory calculation of the complete tetramer within a single unit cell of **Sym-*o*-OMe** or **Sym-*o*-NO$_2$** crystal was performed (Fig. 3g), and the calculated energy gaps of **Sym-*o*-OMe** crystal and **Sym-*o*-NO$_2$** crystal in tetramer forms were 3.389 and 2.347 eV respectively, which supported the fact that **Sym-*o*-NO$_2$** showed more red-shifted solid fluorescence than **Sym-*o*-OMe**. By analyzing the frontier molecular orbital profiles of the tetramer forms of **Sym-*o*-OMe** and **Sym-*o*-NO$_2$**, the core fluorene units contributed less to the LUMO frontier molecular orbitals in comparison with their HOMO frontier molecular orbital contributions for **Sym-*o*-OMe**. While for **Sym-*o*-NO$_2$**, the core fluorene groups had almost no effect on the HOMO and LUMO distributions. Time-dependent density functional theory (TD-DFT) calculations of **Sym-*o*-OMe** crystal and **Sym-*o*-NO$_2$** crystal

in tetramer forms were also carried out to elucidate further the possible solid fluorescence mechanism of **Sym-*o*-OMe** or **Sym-*o*-NO$_2$**. As shown in Fig. S22,† the S$_1$ and S$_2$ excited state energies of **Sym-*o*-OMe** crystal or **Sym-*o*-NO$_2$** crystal in a tetramer form were nearly equivalent, and their S$_3$ excited state energies were also approximate to those of the corresponding S$_1$ and S$_2$ respectively. Therefore, the TD-DFT calculative results indicated that the orbital energy levels of **Sym-*o*-OMe** crystal or **Sym-*o*-NO$_2$** crystal in a tetramer form were close. Thus, diverse electronic transition processes led to analogous energy alterations, which was possibly attributed to the highly symmetric molecular structures of the compounds **Sym-*o*-OMe** and **Sym-*o*-NO$_2$**. Highly symmetric structural systems may exist in multiple excited states with similar energies, thereby resulting in complex emission behaviors. Anisotropic force can modulate luminescence property by altering molecular conformation and packing arrangement, which can affect the orbital interactions. For the tetramer form of **Sym-*o*-OMe** crystal, one predominant S$_0$ → S$_2$ transition showed the oscillator strength (f) of 0.1885, corresponding to 45.6% contribution from the HOMO−3 to LUMO+1 transition and 40.9% contribution from the HOMO−2 to LUMO transition (Table S2†). The HOMO−3, LUMO+1, HOMO−2, and LUMO electron densities were predominantly distributed at the triphenylamine groups, which suggested that blue-green fluorescence of the pristine solid **Sym-*o*-OMe** should originate from the local excited state emission. Under the anisotropic force stimulation, the tetrameric conformation and packing arrangement of **Sym-*o*-OMe** underwent variations, leading to the alteration of orbital interactions and the increase of the energy gap differences among the S$_1$, S$_2$, and S$_3$ excited states, which facilitated the predominant S$_0$ → S$_1$ transition in compliance with Kasha's Rule. As a consequence, solid **Sym-*o*-OMe** showed a red-shift fluorescence upon mechanical stimulation. Additionally, the force-triggered high-contrast tricolored solid fluorescence feature of **Sym-*o*-OMe** might be associated

with multi-orbital transition contributions to its excited states (Fig. S22†). As for the tetramer form of **Sym-o-NO$_2$** crystal, one predominant S$_0 \rightarrow$ S$_2$ transition showed the f value of 0.0007, corresponding to 69.7% contribution from the HOMO−2 to LUMO+1 transition and 19.7% contribution from the HOMO to LUMO+1 transition (Table S2†). The HOMO−2, LUMO+1, and HOMO electron densities were predominantly distributed at the different units, which indicated that the orange-yellow fluorescence of the pristine solid **Sym-o-NO$_2$** was derived from charge transfer (CT) state emission. The S$_1$ and S$_2$ excited state energies of **Sym-o-NO$_2$** crystal in a tetramer form were identical, and the corresponding f values were also approximate (Fig. S22†). Consequently, **Sym-o-NO$_2$** demonstrated similar solid-state fluorescence regardless of whether the S$_0 \rightarrow$ S$_1$ or S$_0 \rightarrow$ S$_2$ transition dominated the emission process, which supports the fact that solid **Sym-o-NO$_2$** exhibits an inconspicuous three-color mechanofluorochromism. When the solid samples of luminogens **Sym-o-OMe** and **Sym-o-NO$_2$** were subjected to vigorous grinding, the dominant emission would obey Kasha's Rule, and the contribution of excited states primarily arose from the HOMO to LUMO transition. For the tetramer form of **Sym-o-OMe** or **Sym-o-NO$_2$** crystal, the HOMO and LUMO electron densities were distinctly distributed at different regions of the tetramer (Fig. S22†), and thus the CT state emission was responsible for the red fluorescence of solid **Sym-o-OMe** or **Sym-o-NO$_2$** after heavy grinding. Compared with **Sym-o-OMe**, **Sym-o-NO$_2$** demonstrated more and multiple stronger intermolecular interactions (Fig. 3e and f, S23 and Table S3†) and the more crowded molecular packing (Fig. 3h and i), which made it more difficult for **Sym-o-NO$_2$** to effectively to regulate the molecular arrangement mode through mechanical stimulation. Indeed, the inconspicuous three-color mechanofluorochromism was observed for the luminogen, **Sym-o-NO$_2$** (Fig. S24†).

Sym-m-OMe and **Sym-p-OMe**, capable of showing high-contrast three-color mechanofluorochromic responses, have significant value in the anticounterfeiting field, and three advanced anticounterfeiting systems were ingeniously developed. First, a multilayer anticounterfeiting system was successfully constructed by applying force-induced tricolored solid fluorescence to **Sym-p-OMe** and integrating the colored quick response (QR) code, binary American Standard Code for Information Interchange (ASCII) code, Morse code, and Caesar cipher techniques. As shown in Fig. 4, one QR code containing spurious information "efde-zlkqoxpq cirlobpzbkzb ptfqze" was generated based on IEC 18004, and a transparent diaphragm was used as the base, with the formed QR code engraved on it. The carved scratches with grooves were neatly filled with green fluorescent powder of **Sym-p-OMe**. Under 365 nm UV light, the information "efde-zlkqoxpq cirlobpzbkzb ptfqze" was extracted by scanning the green emissive QR code. Upon slight grinding, the first, second, fifth, sixth, and seventh small squares from left to right on the seventh row, as well as the third, fourth, and fifth small squares from left to right on the tenth row of the QR code, their green fluorescence of the corresponding small squares was changed into yellow fluorescence. Subsequently, the heavy grinding of the third, fourth, and eighth small squares from left to right on the seventh row, as well as the first

and second small squares from left to right on the tenth row of the QR code, caused the fluorescence to change from green to red. The yellow and red fluorescent squares on the seventh row were designated as binary codes "0" and "1," respectively, and the information "1" was obtained from the 8-bit binary codes in accordance with the principle of ASCII codes. However, the yellow and red fluorescent squares on the tenth row were set to Morse codes "—" and "·" respectively, and the information "2" was extracted from the combinatorial 5-bit Morse codes according to the Morse code meter. Information "1" plus information "2" gave a character offset of "3". Based on the Caesar cipher table, the final password information "high-contrast fluorescence switch" was deciphered by the integration of the initial information "efde-zlkqoxpq cirlobpzbkzb ptfqze" and a character offset of "3".

Three-dimensional (3D) codes, consisting of colored patterns, are promising emerging information storage medium.[56] Relying on the unique color dimension that can be used for additional information storage, 3D-colored codes allow us to encode more information compared with 1D barcodes and 2D codes. As presented in Fig. 5, the second anticounterfeiting system was constructed based on the 3D-colored code. Luminogen **Sym-m-OMe** showed force-triggered yellow-green-to-green-to-red bidirectional high-contrast fluorescence switching nature, which provided a basis for developing dynamic and high-efficiency 3D-colored code-based anticounterfeiting system applying **Sym-m-OMe**. The 3D-colored code containing encrypted information "bidirectional high-contrast mechanofluorochromism" was formed *via* the registered COLORCODE APP program. The specific yellow-green, green, and red blocks of the generated 3D-colored code could be realized by different solid-state fluorescent **Sym-m-OMe** powders. In contrast, the remaining black blocks could be replaced with nonfluorescent commercial carbon powder. Furthermore, the force-controllable yellow-green-to-green-to-red three-color fluorescence feature of **Sym-m-OMe** enabled this constructed 3D-colored code-based anticounterfeiting system to accomplish dynamic information encryption. More concretely, a transparent diaphragm with 25 minor square grooves was chosen as the base. The five black blocks were covered with carbon powder, while the remaining 20 blocks were neatly filled with the as-prepared yellow-green fluorescent **Sym-m-OMe** powder. No information was obtained by scanning the initial 3D code under the UV irradiation of 365 nm or sunlight by using the COLORCODE APP software. The encrypted information was still not extracted by scanning the processed 3D code in which the six specific yellow-green fluorescent blocks at the first row first column, second row second column, third row first column, third row fifth column, fourth row first column, and fifth row fourth column was converted into green emissive blocks by slight grinding. Indeed, the hidden information "bidirectional high-contrast mechanofluorochromism" could only be deciphered by scanning the further processed 3D code in which the nine specific blocks at the first row fifth column, second row fifth column, third row third and fourth columns, fourth row second, third and fifth columns, fifth row first and fifth columns among the remaining fourteen yellow-green emissive

blocks were transformed into red fluorescent blocks by heavy grinding.

Last, a multilayer anticounterfeiting system relying on pigpen cipher and ternary code for information decryption was established. As can be seen in Fig. 6, three sets of patterns composed of pigpen ciphers, which were located at the top, on the left side, and on the right side, respectively, were engraved on one transparent diaphragm. The grooves of carved scratches were padded with green fluorescent solid **Sym-*p*-OMe**. According to the rule of the pigpen cipher, the password information "GRADUALLY BATHOCHROMIC THREE COLORS" formed by three sets of patterns could be deciphered by following the order from the top to the left and then to the right. The force-induced green-to-yellow-to-red tricolor solid fluorescence changes of **Sym-*p*-OMe** provided the possibility for further information encryption using ternary code and integrating the two sets of patterns from both the left and right sides as one research subject. Slight grinding of the images at the first row first column, first row third column, second row first column, second row third column, third row first column, third row third column, and fourth row first column, and the fluorescence of these images changed from green to yellow. Next, the heavy grinding of the images at the first row second column, first row fourth column, second row second column, third row second column, third row fourth column, fourth row second column, fourth row third column, and fourth row fourth column resulted in their fluorescence changes from green to red. For the first four rows, the green, yellow, and red fluorescent images were designated as ternary codes "0", "1", and "2", respectively, and the second layer information, "2025", was deciphered by following the order from top to bottom based on Ternary code table. Ultimately, the complete password information "GRADUALLY BATHOCHROMIC THREE COLORS 2025" was acquired by the combination of information "GRADUALLY BATHOCHROMIC THREE COLORS" and "2025".

Conclusions

15 symmetric luminogens were prepared through a molecular engineering strategy comprised of isomeric and substituent engineering based on the core organic moiety 4,4′-((9*H*-fluoren-9-ylidene)methylene)bis(*N*,*N*-diphenylaniline), and 11 luminogens featuring with anisotropic force-manipulatable tricolored solid fluorescence were developed. Impressively, 9 luminogens displaying scarce anisotropic force-triggered high-contrast three-color fluorescence switching characteristics were efficiently screened out. Among them, four fluorogenic compounds, including our previously reported **Sym-*o*-CF₃**, showed force-dependent hypso- and bathochromic bidirectional high-contrast fluorescence responses. Simultaneously, the remaining five luminogens belonged to force-controllable gradually bathochromic high-contrast tricolor fluorescence switching molecules. Based on the anisotropic force-triggered contrasting three-color solid fluorescence properties of the newly prepared representative luminogens **Sym-*p*-OMe** and **Sym-*m*-OMe**, three advanced modes of high-security information anticounterfeiting were elaborately designed. This work

not only discovers a series of relatively uncommon anisotropic force-induced high-contrast three-color fluorescence molecular switches through a promising molecular engineering strategy but also inspires innovative anticounterfeiting applications of force-responsive intelligent luminogens.

Data availability

All experimental and characterization data are available in the ESI.† Crystallographic data of **Sym-*o*-OMe** and **Sym-*o*-NO₂** have been deposited in the Cambridge Crystallographic Data Centre as supplemental publications CCDC 2432608 (**Sym-*o*-OMe**) and CCDC 2432609 (**Sym-*o*-NO₂**).

Author contributions

Z. C. directed the project; Z. C. wrote the manuscript; Z. C. conceived the work; Z. C. designed the experiments; Z. C., Y. Z., Y. Y., D. D., and Y. Y. performed the synthesis experiments involving 15 symmetric luminogens; Z. C. and Y. Z. performed the tests of photophysical properties of 15 symmetric luminogens; Z. C., Y. Y., C. F., and G. L. cultivated the single crystals and analysed the crystal data; Z. C. and Y. Z. constructed three advanced information anticounterfeiting systems; Z. C. and S. P. supervised this work. All authors approved the final version of the manuscript.

Conflicts of interest

There are no conflicts to declare.

Acknowledgements

Notes and references

1 Z. Xie, C. Chen, S. Xu, J. Li, Y. Zhang, S. Liu, J. Xu and Z. Chi, *Angew. Chem., Int. Ed.*, 2015, **54**, 7181–7184.

2 L. Wilbraham, M. Louis, D. Alberga, A. Brosseau, R. Guillot, F. Ito, F. Labat, R. Métivier, C. Allain and I. Ciofini, *Adv. Mater.*, 2018, **30**, 1800817.

3 T. Suzuki, H. Okada, T. Nakagawa, K. Komatsu, C. Fujimoto, H. Kagic and Y. Matsuo, *Chem. Sci.*, 2018, **9**, 475–482.

4 P. Josse, M. Allain, J. P. Calupitan, Y. Jiang, C. Cabanetos and J. Roncali, *Adv. Opt. Mater.*, 2020, **8**, 2000420.

5 D. Sun, Y. Wu, X. Han and S. Liu, *Nat. Commun.*, 2023, **14**, 4190.

6 S. S. Rana and J. Choudhury, *Angew. Chem., Int. Ed.*, 2024, **63**, e202406514.

7 X. Zheng, X. Liu, L. Liu, X. Li, S. Jiang, C. Niu, P. Xie, G. Liu, Z. Cao, Y. Ren, Y. Qin and J. Wang, *Angew. Chem., Int. Ed.*, 2022, **134**, e202113073.

8 J. Zhang, B. He, W. Wu, P. Alam, H. Zhang, J. Gong, F. Song, Z. Wang, H. H. Y. Sung, I. D. Williams, Z. Wang, J. W. Y. Lam and B. Z. Tang, *J. Am. Chem. Soc.*, 2020, **142**, 14608–14618.

9 Y. Wang, Y. Wang, L. Wei, A. Li, Y. Fang, L. Li, Q. Li and K. Wang, *Chem. Eng. J.*, 2025, **507**, 160849.

10 Y. Li, W. Huang, J. Yong, S. Huang, Y. Li, Y. Liu and D. Wu, *New J. Chem.*, 2018, **42**, 12644–12648.

11 X. Ma, X. Xu, F. Duan, W. Huang, Q. Chen and D. Wu, *Adv. Optical Mater.*, 2022, **10**, 2101461.

12 Y. Matsunaga and J.-S. Yang, *Angew. Chem., Int. Ed.*, 2015, **54**, 7985–7989.

13 X. Zhang, X. Huang, X. Gan, Z. Wu, J. Yu, H. Zhou, Y. Tian and J. Wu, *Sens. Actuators, B*, 2017, **243**, 421–428.

14 H. Wu, W. Wu, L. Hu, J. Zhu, Q. Li, Y. Gao, Y. Wei, G. Jiang and Y. Yang, *Chem. Eng. J.*, 2023, **469**, 143781.

15 Y. Aoyama, S. Ito and K. Tanaka, *Macromolecules*, 2024, **57**, 6559–6567.

16 R. Nishimura, Y. Kobayashi, H. Sotome, H. Miyasaka and M. Morimoto, *Adv. Opt. Mater.*, 2024, **12**, 2400143.

17 G. Huang, Q. Xia, W. Huang, J. Tian, Z. He, B. S. Li and B. Z. Tang, *Angew. Chem., Int. Ed.*, 2019, **131**, 17978–17983.

18 Y. Guo, A. Wu, Q. Zhang, M. Zhao, Y. Gong, S. Liu, M. Khan, H. Song, J. Yoon and Q. Hu, *Chem. Eng. J.*, 2024, **497**, 154721.

19 M. Okazaki, Y. Takeda, P. Data, P. Pander, H. Higginbotham, A. P. Monkmanb and S. Minakata, *Chem. Sci.*, 2017, **8**, 2677.

20 V. Kachwal and I. R. Laskar, *Topics Curr. Chem.*, 2021, **12**, 4243.

21 Y. Shen, B. Wang, P. Wang, Y. Chen, Z. Xu, W. Huang and D. Wu, *Inorg. Chem.*, 2024, **63**, 12073–12080.

22 H. Sun, S. Shen, C. Li, W. Yu, Q. Xie, D. Wu and L. Zhu, *Adv. Funct. Mater.*, 2025, **35**, 2415400.

23 H. Sun, Z. Yu, C. Li, M. Zhang, S. Shen, M. Li, M. Liu, Z. Li, D. Wu and L. Zhu, *Angew. Chem., Int. Ed.*, 2025, **64**, e202413827.

24 Z. Chi, X. Zhang, B. Xu, X. Zhou, C. Ma, Y. Zhang, S. Liu and J. Xu, *Chem. Soc. Rev.*, 2012, **41**, 3878–3896.

25 K. Nagura, S. Saito, H. Yusa, H. Yamawaki, H. Fujihisa, H. Sato, Y. Shimoikeda and S. Yamaguchi, *J. Am. Chem. Soc.*, 2013, **135**, 10322–10325.

26 B. Li, K. Seth, B. Niu, L. Pan, H. Yang and H. Ge, *Angew. Chem., Int. Ed.*, 2018, **130**, 3459–3463.

27 R. Gavale, F. Khana and R. Misra, *J. Mater. Chem. C*, 2025, **13**, 1063–1129.

28 Y. Sun, K. Wang, X. Huang, S. Wei, E. Contreras, P. K. Jain, L. M. Campos, H. J. Kulik and J. S. Moore, *J. Am. Chem. Soc.*, 2024, **146**, 27117–27126.

29 F. Khan, A. Ekbote, G. Singha and R. Misra, *J. Mater. Chem. C*, 2022, **10**, 5024–5064.

30 F. Khana and R. Misra, *J. Mater. Chem. C*, 2023, **11**, 2786–2825.

31 W. Z. Yuan, Y. Tan, Y. Gong, P. Lu, J. W. Y. Lam, X. Y. Shen, C. Feng, H. H.-Y. Sung, Y. Lu, I. D. Williams, J. Z. Sun, Y. Zhang and B. Z. Tang, *Adv. Mater.*, 2013, **25**, 2837–2843.

32 J.-C. Yang, Z. Fu, H. Ma, T. Wang, Q. Li, K. Wang, L. Wu, P. Chen, H.-T. Feng and B. Z. Tang, *ACS Materials Lett.*, 2023, **5**, 1441–1449.

33 J. Song, Y. Zhou, Z. Pan, Y. Hu, Z. He, H. Tian and X. Ma, *Matter*, 2023, **6**, 2005–2018.

34 J. Wang, B. Yue, X. Jia, R. Cao, X. Niu, H. Zhao, J. Li and L. Zhu, *Chem. Commun.*, 2022, **58**, 3517–3520.

35 Y. Ai, Y. Li, M. H.-Y. Chan, G. Xiao, B. Zou and V. W.-W. Yam, *J. Am. Chem. Soc.*, 2021, **143**, 10659–10667.

36 T. Mutai, T. Sasaki, S. Sakamoto, I. Yoshikawa, H. Houjou and S. Takamizawa, *Nat. Commun.*, 2020, **11**, 1824.

37 Z. Ma, M. Teng, Z. Wang, S. Yang and X. Jia, *Angew. Chem., Int. Ed.*, 2013, **52**, 12268–12272.

38 W. Guo, M. Wang, L. Si, Y. Wang, G. Xia and H. Wang, *Chem. Sci.*, 2023, **14**, 6348–6354.

39 Y. Yin, Q. Guan, Z. Chen, D. Deng, S. Liu, Y. Sun and S. H. Liu, *Sci. Adv.*, 2024, **10**, eadk5444.

40 C. Wang and Z. Li, *Mater. Chem. Front.*, 2017, **1**, 2174–2194.

41 M. Yang, Z. Zeng, J. W. Y. Lam, J. Fan, K. Pu and B. Z. Tang, *Chem. Soc. Rev.*, 2022, **51**, 8815–8831.

42 G. Fei, S. Li, Y. Liu, J. B. Carney, T. Chen, Y. Li, X. Gao, J. Chen, P. Chen, Y. Yue, K. Bao, B. Tang and G. Chen, *Chem. Commun.*, 2024, **60**, 10–25.

43 D. Xu, M. Wang, R. Huang, J. F. Stoddart and Y. Wang, *J. Am. Chem. Soc.*, 2025, **147**, 4450–4458.

44 M. Jin and H. Ito, *J. Photoch. Photobio. C.*, 2022, **51**, 100478.

45 Q. Liao, Q. Li and Z. Li, *Adv. Mater.*, 2023, 2306617.

46 K. Huang, L. Song, K. Liu, A. Lv, M. Singh, K. Shen, J. Shen, J. Wang, H. Wang, H. Shi, H. Ma, M. Gu, G. Sun, W. Yao, Z. An and W. Huang, *npj Flexible Electron.*, 2021, **5**, 21.

47 W.-J. Guo, S. Yan, L. Chen, L. Qiao, S. Xu, T. Qi, B. Liu and H.-Q. Peng, *Adv. Funct. Mater.*, 2024, **34**, 2406888.

48 J. Wu, Y. Cheng, J. Lan, D. Wu, S. Qian, L. Yan, Z. He, X. Li, K. Wang, B. Zou and J. You, *J. Am. Chem. Soc.*, 2016, **138**, 12803–12812.

49 G. Yang, W.-X. Zhao, J.-Y. Cao, Z.-M. Xue, H.-T. Lin, S.-H. Chen, T. Yamato, C. Redshaw and C.-Z. Wang, *Chem. Commun.*, 2024, **60**, 3966–3969.

50 Q. Wang, Y. Xu, T. Huang, Y. Qu, J. Xue, B. Liang and Y. Wang, *Angew. Chem., Int. Ed.*, 2023, **62**, e202301930.

51 G. Ye, Y. Yang, W. Yuan, J. Gu, S. Li, Q. Li and Z. Li, *ACS Materials Lett*, 2024, **6**, 4639–4648.

52 T. Seki, Y. Takamatsu and H. Ito, *J. Am. Chem. Soc.*, 2016, **138**, 6252–6260.

53 P. S. Hariharan, V. K. Prasad, S. Nand, A. Anoop, D. Moon and S. P. Anthony, *Cryst. Growth Des.*, 2017, **17**, 146–155.

54 H.-W. Zheng, S. Li, M. Wu, Y. Kang, J.-B. Li, Q.-F. Liang, X.-J. Zheng, D.-C. Fang and L.-P. Jin, *J. Mater. Chem. C*, 2020, **8**, 4246–4252.

55 H.-W. Zheng, M. Wu, D.-D. Yang, Q.-F. Liang, J.-B. Li and X.-J. Zheng, *Inorg. Chem.*, 2021, **60**, 11609–11615.

56 X. Ji, R.-T. Wu, L. Long, X.-S. Ke, C. Guo, Y.-J. Ghang, V. M. Lynch, F. Huang and J. L. Sessler, *Adv. Mater.*, 2018, **30**, 1705480.